Assessment of carbon dioxide capture by precipitating potassium taurate solvent

Stefania Moioli[a,b], Minh T. Ho[b], Dianne E. Wiley[b], Laura A. Pellegrini[a]

[a]*GASP, Group of Advanced Separation Processes and GAS Processing, Dipartimento di Chimica, Materiali e Ingegneria Chimica "Giulio Natta", Politecnico di Milano, Piazza Leonardo da Vinci 32, I-20133 Milano, Italy*

[b]*The University of Sydney, School of Chemical and Biomolecular Engineering, NSW 2006, Australia*

Corresponding Author: stefania.moioli@polimi.it

Abstract

One of the most mature technologies for removal of carbon dioxide from gaseous streams is chemical absorption. Among these, aqueous solutions of amino acids have been considered because of the advantages associated with their being precipitating solvents. This paper presents detailed analyses of the performance of the potassium taurate absorption system by means of a rigorous simulation in a commercial process software (ASPEN Plus®). The profiles of temperature, heat transfer, compositions, and molar flows of carbon dioxide and water have been examined. The operating line and the equilibrium curve for different lean loadings of the solvent are reported and show that the minimium reboiler duty occurs at a lean loading of 0.27. Examination of the influence of the solid-liquid separator on the reboiler duty shows that a recycle split fraction of 0.2 results in the lowest reboiler duty. Different minimum temperature approaches in the lean-rich cross heat exchanger have also been investigated.

1. Introduction

Since the last century, emissions of greenhouse gases, mainly carbon dioxide (Gupta et al., 2003), from combustion of fossil fuels have significantly increased, with values in 2014 more than 55% the value in 1990 (Copernicus, 2015), and contributing about 78% of the total greenhouse gas emissions (GHG) (Metz et al., 2005), thereby causing the Earth's temperature to rise. Several techniques have been considered to minimize emissions of carbon dioxide (Mac Dowell et al., 2017), with one of the most commonly applied being the reduction of acid gases from flue gas exiting power plants before sending it to the atmosphere.

Traditionally, chemical absorption with an amine solvent is used to remove acid gases (Kohl and Nielsen, 1997). However recently alternative solvents such as amino acid solvents (Aronu et al., 2013; Lerche, 2012; Majchrowicz, 2014; Majchrowicz et al., 2009; Simons et al., 2010; Vaidya et al., 2010; van Holst et al., 2009) have started to be studied for possible application to carbon dioxide removal. They can be used as additional components in traditional solvents to enhance the absorption process, such as in the Alkacid process (Kohl and Nielsen, 1997), or as the main solvent in the aqueous solution.

This class of solvent is under consideration because of its potential to be economically advantageous in comparison with traditional amines. The main advantage is due to the solid precipitation, which, according to the Le Chatelier's principle, favors the absorption of carbon dioxide and therefore enhances the overall removal process. For this reason, a number of research investigations have been carried out, focusing primarily on the experimental investigation of the characteristics of these systems when applied to CO_2 removal.

Majochrowicz et al. (Majchrowicz et al., 2009) showed that the precipitate composition depends on the type of amino acid salt and may be in the form of pure amino acid, as in the case of taurine, or more complex species containing also carbon dioxide, as in the case of

proline, sarcosine and β-alanine. Aronu et al. (Aronu et al., 2013) found that the reaction rate for these systems decreases significantly as the equilibrium condition is approached and that the potassium salt of the amino acid generally shows better reaction kinetics than the sodium salt. Experimental data of density and viscosity and studies of diffusivities have been performed by Kumar et al. Kumar et al. (2001), who then focused also on the crystallization of the system (Kumar et al., 2003a), on the solubility of carbon dioxide (Kumar et al., 2003b) and on the kinetics of reaction for absorption of CO_2 (Kumar et al., 2003c). Wei et al. (Wei et al., 2014; Wei et al., 2013) determined the reaction rate constants for the formation of carbamate in the range of temperatures between 323 K and 353 K, finding that at high temperatures a fast carbon dioxide absorption rate may be obtained.

Modeling of this type of system started to be considered only recently, and very few models are available in the literature. A Kent-Eisenberg model has been considered by Aftab et al. (Aftab et al., 2018) for the aqueous sodium β-alanine system, while for the description of the potassium taurate system an empirical model has been created by Sanchez-Fernandez et al. (Sanchez-Fernandez, 2013) on the basis of collected experimental data. The need for accurate thermodynamic-based models has been recently outlined in a review on the employment of amino acid salt solutions for removal of carbon dioxide (Zhang et al., 2018).

Moioli et al. developed a thermodynamic model in ASPEN Plus® for the simulation of CO_2 absorption by potassium taurate solvent (Ho et al., 2019; Moioli et al., 2017), which had not been performed in the previous literature. Because of limitations of data in the simulator database, components not available were added to the software and a user-customized model for the best description of the vapor-liquid-solid equilibrium and the reaction constants has been developed and validated by comparison with experimental data available in the literature. Details are available in Moioli et al. (Moioli et al., 2018).

Sanchez-Fernandez and Goetheer (Sanchez-Fernandez and Goetheer, 2011) developed a conceptual design of the DECAB process, showing that there is significant potential to reduce energy consumption by employing different schemes for regeneration and by selecting the appropriate amino acid solvent. The process involving potassium taurate solution is characterized by a low energy consumption, and in addition has the key advantages of absence of emissions to the air and reduced environmental impact. In a high level assessment of the process, Raksajati et al. (Raksajati et al., 2016) identified key areas of the system design for cost reduction including the use of a packed column for absorption as well as the use of advanced heat exchanger integration.

This paper employs the user customized model of Moioli at al. (Moioli et al., 2018) for carrying out a rate-based simulation to develop an improved understanding of some key factors affecting the performance of the potassium taurate absorption process including a high level comparison to some key competitor solvent systems. This tool provides the ability to include more rigorous interactions and investigate a larger range of parameters than can be completed based on more simple models as has been previously reported in the literature.

By performing a rate-based simulation of the process, the influence of the lean loading and of the solid-liquid separator on the energy requirements as well as on key features of the system such as the temperature profile, heat transfer and mass tranfer within the absorption column is evaluated. In addition, the effect of the temperature approach in the cross heat exchanger and the absorber height on the L/G ratio are studied in order to understand if analogies to traditional amine systems may be applied.

2. Methodology

2.1. Description of the process

The schematic of the potassium taurate process is shown in Figure 1. The layout is similar to the one for traditional amine scrubbing but with some additional and optional equipment. Because of its limited solubility, at the saturation point taurine precipitates as the pure compound. The set of chemical reactions includes the formation of solid taurine (Section 2.2). According to Le Chatelier's principle, taurine precipitation shifts the reaction equilibrium towards the formation of more products, resulting in a higher amount of carbon dioxide being reacted and absorbed. A slurry is obtained at the bottom of the absorption column consisting of solid taurine and a liquid mixture of molecular and ionic species in water. The slurry is pumped to the optional units before being heated in the cross heat exchanger to dissolve all the solids before entering the desorption column. The high heat content present in the lean solvent exiting the regenerator is recovered in the cross heat exchanger and transferred to the cold rich solution entering the desorber as pre-heat and to achieve energy savings in the reboiler.

The solid-liquid separator and the dissolution heat exchanger are optional units.

The separator creates two streams, one of supernatant liquid and one of concentrated slurry. The flowrate of the two streams is determined by the recycle split fraction (RSF), which is defined as the amount of liquid stream recycled back to the absorber without undergoing regeneration (stream (5)) over the total amount of liquid fed to the solid-liquid separator (stream (4)). Because of the presence of solid taurine in the slurry, the two streams exiting the solid-liquid separator have different compositions and pH with the supernatant having a lower ratio of total taurine to total potassium than the slurry. In particular, the slurry stream is enriched in amino acid and has a lower pH than the rich stream before solid-liquid separation (stream 4). The lower pH favors desorption by producing a higher equilibrium partial pressure of carbon

dioxide at any given loading (Kumar et al., 2003b; Sanchez Fernandez et al., 2013), thus reducing the energy requirements for regeneration. The lean-rich heat exchanger and optional dissolution heat exchanger operate in a manner that ensures that there are no solids present in the regeneration section of the process. The supernatant is recycled back to the absorption column without being regenerated, being mixed with the renegerated lean stream from the regenerator prior to entering the absorption column.

The dissolution heat exchanger heats the concentrated slurry up to the dissolution temperature to dissolve the solid taurine before entering the cross heat exchanger. If the dissolution heat exchanger is not present, all of the solids must be dissolved in the cross heat exchanger. Heat exchangers for dissolution of solids are generally characterized by good values of heat flux (Perry and Green, 1997), even when the solid cake is present. However, in this system, it is assumed that a cake of solids does not form within the cross heat exchanger due to the low amount of solids (lower than about 5% on a weight basis). Rather it is assumed that the stream circulates as a liquid slurry. Thus, issues with regards to handling of solids in the heat exchangers should not be significant in this case. Detailed analyses and experiments should be undertaken as part of future research to check the accuracy of this assumption.

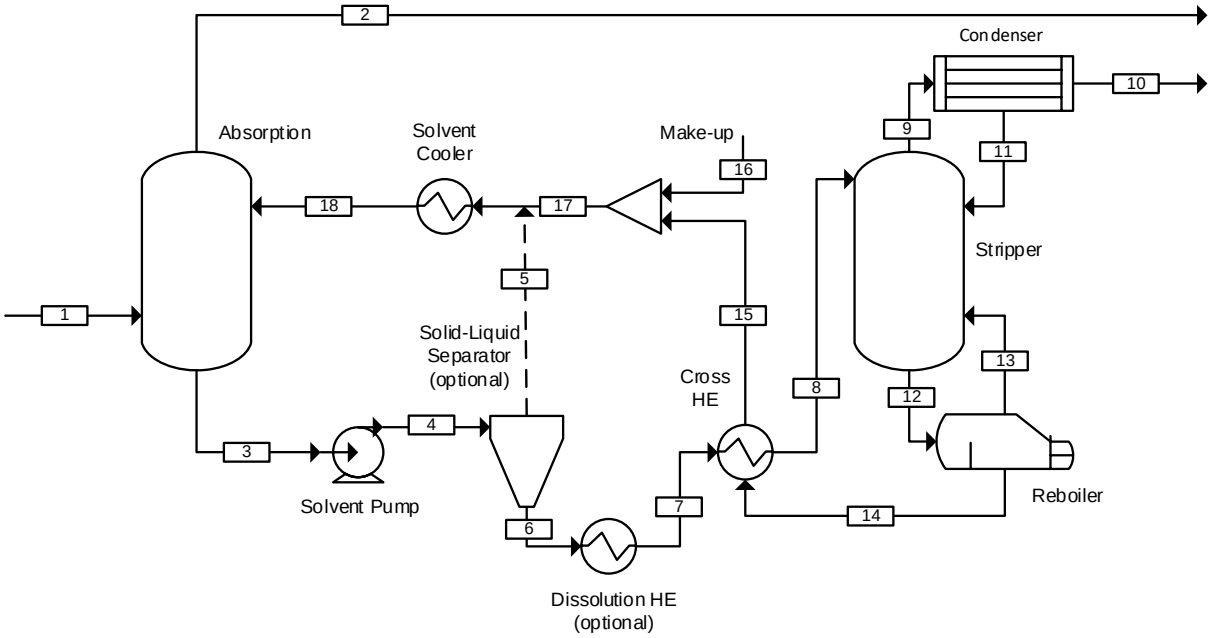

Figure 1. Scheme of the potassium taurate process.

2.2. Thermodynamic model

The commercial software ASPEN Plus® has been customized for the simulation of the potassium taurate system. The simulator is provided by default with the molecular species water, KOH, carbon dioxide, nitrogen and oxygen and with the ionic species formed by reactions of these compounds in aqueous solution. It is not provided with the ionic species of taurine. In addition, all the thermodynamic parameters related to taurine, both in the molecular and in the ionic form, and to interactions of the other species with these compounds, are not present. Our previous work (Moioli et al., 2018; Moioli et al., 2019) describes how we developed and added this information.

Generally, the potassium taurate absorption process can be considered as being close to the amine scrubbing one, since both of them are chemical reaction processes dealing with the formation of a carbamate and with similar aspects regarding the carbon dioxide absorption (though precipitation does not occur).

The set of chemical equilibrium reactions involving solid taurine formation is:

$$TAUSOLID(s) \overrightarrow{\leftarrow} TAURINE \quad (1)$$

$$TAUH^+ + H_2O \overrightarrow{\leftarrow} TAURINE + H_3O^+ \quad (2)$$

$$TAURINE + H_2O \overrightarrow{\leftarrow} TAU^- + H_3O^+ \quad (3)$$

$$2H_2O \overrightarrow{\leftarrow} H_3O^+ + OH^- \quad (4)$$

$$CO_2 + 2H_2O \overrightarrow{\leftarrow} HCO_3^- + H_3O^+ \quad (5)$$

$$HCO_3^- + H_2O \overrightarrow{\leftarrow} CO_3^{2-} + H_3O^+ \quad (6)$$

$$CO_2 + TAU^- + H_2O \overrightarrow{\leftarrow} TAUCOO^{2-} + H_3O^+ \quad (7)$$

$$KOH \rightarrow K^+ + OH^- \quad (8)$$

with *TAU*$^-$ referring to the deprotonated taurine, *TAUH*$^+$ to the protonated taurine and *TAUCOO*$^-$ to the carbamate.

In addition, another set of chemical reactions that does not include solids has been defined for rate-based simulation of the absorption and regeneration units that still takes into account the influence of the solid phase on the equilibrium. This is a necessary theoretical artefact used in the simulations because the rate-based simulation tool in the simulation package is not able to accommodate solids. The Electrolyte-NRTL (Chen et al., 1979; Chen et al., 1982; Chen and Evans, 1986; Mock et al., 1986) model has been used for estimating the phase behavior of the system, which is strongly non-ideal because of the presence of electrolytes and ions. A detailed description of the thermodynamic system and of the chemical equilibrium reactions is reported in Moioli et al. (Moioli et al., 2018), where the equilibrium constants and the interaction parameters have been determined and checked against available experimental data.

2.3. Process simulation

By analogy to amine scrubbing, absorption is assumed to be a rate controlled phenomenon, with mass and heat transfer being kinetically limited processes (Abu Zahra, 2009; Kucka et al., 2003; Zhang et al., 2009). The absorber has therefore been modeled as a rate-based column with kinetic-controlled reactions while the regenerator has been modeled as a rate-based column with chemical equilibrium reactions, connected to a condenser and a reboiler both assumed as equilibrium units (Plaza, 2012). The kinetic parameters for the forward and backward reaction for carbamate formation are taken from Wei et al. (Wei et al., 2014) while parameters for the forward and backward reaction for bicarbonate formation are available in ASPEN Plus® (AspenTech, 2016).

The internals of the absorption and desorption columns have been assumed to be an hypothetical packing suitable for treating slurry systems with a surface area similar to that of the commercial packing Mellapak 250X (Raksajati et al., 2016). At the current point in time, there are few packings available that are known to handle precipitates. Devries (Devries, 2014) performed some experimental tests for the effect of $KHCO_3$ precipitation on absorption of carbon dioxide and showed that their structured packing did not plug during the tests. The US EPA (EPA, 2014) has reported that mobile bed scrubbers packed with low density plastic spheres are less susceptible to plugging by solids because of the increased movement of the packing material.

The simulation of the scheme with solid-liquid separator has been carried out iteratively. By starting with a defined lean loading for stream (18) of Figure 1, and selecting a fixed recycle split fraction, a value for stream (5) and stream (6) was found and the total circulating flowrate of the solvent was adjusted to make the absorber achieve the desired 90% CO_2 removal.

Iterations were completed until convergence was reached *i.e.* the change in flowrate of all components in stream (18) was no more than 1×10^{-4} between iterations.

2.4. Model validation

The thermodynamic model has been validated previously (Moioli et al., 2018), showing a good representation of the phase equilibrium of the system (Figure 2) and a good agreement between calculated and experimental data, with errors in the order of maximum 10%. A comparison of the simulation results from this paper with the results obtained from a different semi-empirical model previously developed (Sanchez Fernandez et al., 2013) shows that the models obtain similar trends.

a)

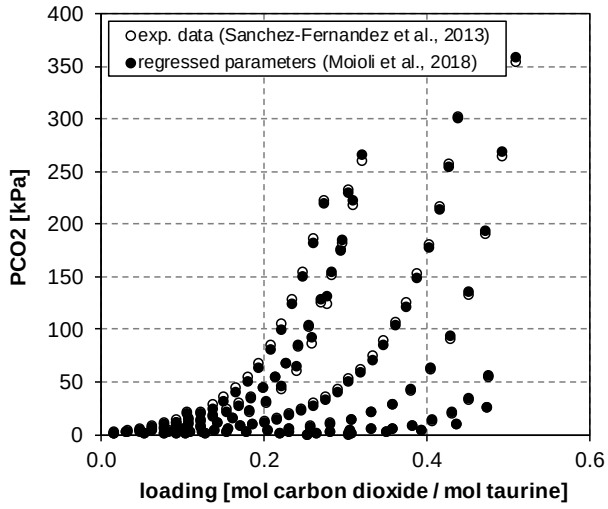

b)

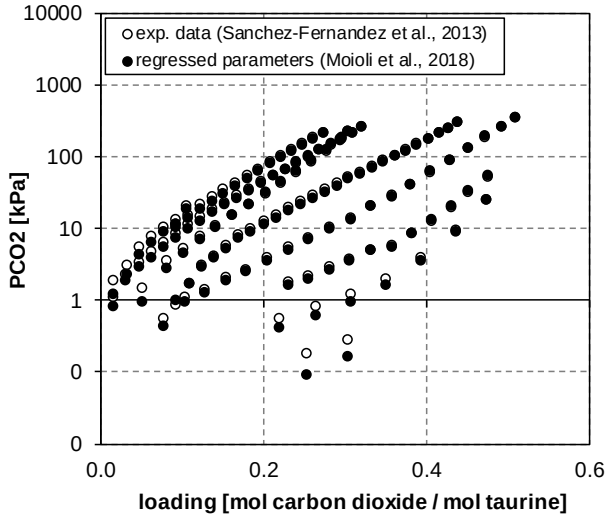

Figure 2. Comparison between calculated and experimental data for solubility of carbon dioxide in potassium taurate solution at fixed temperature and liquid phase composition represented in a) normal plot and in b) log-scale plot.

2.5. Case studies

This paper considers post-combustion of carbon dioxide from the flue gas of a super-critical black coal-fired power plant with a power output of 500 MW (Raksajati et al., 2016). The flowrate and composition of the flue gas stream is presented in Table 1. The removal rate for carbon dioxide is fixed at 90%.

Table 1. Characteristics of the flue gas.

Total Flow [kmol/sec]	19.60
mole fraction	
water	0.0700
carbon dioxide	0.1300
nitrogen	0.7500
oxygen	0.0500

Table 2 shows the fixed variables used for the key process units in the simulations. In rate-based calculations column dimensions need to be given as an input. For the simulation they have been taken from Raksajati et al. (Raksajati et al., 2016), who estimated the column dimensions for the same flue gas stream. The diameter can also be estimated in the simulator with the "Pack Design" tool, based on correlations by ASPEN Plus® typical of each packing and including the height of the column. A diameter of 19.998 m was estimated for the absorber from the simulation in ASPEN Plus®, and cross-checked with the one reported in Table 2, which shows the input variables employed in this paper.

Table 2. Input variables for key process units and process streams.

Variable	**Value**
absorber pressure [atm]	1
absorber diameter [m]	20.7 (from (Raksajati et al., 2016))
absorber height [m]	20 (from (Raksajati et al., 2016))
absorber packing	Mellapak 250X
temperature of the solid/liquid separator [°C]	40
outlet temperature of the dissolution heat exchanger [°C]	76
minimum $\Delta T_{approach}$ in the lean-rich heat exchanger [°C]	10
condenser temperature [°C]	40
regenerator pressure [atm]	1.8
regenerator diameter [m]	16.6 (from (Raksajati et al., 2016))
regenerator height [m]	17.6 (from (Raksajati et al., 2016))
regenerator packing	Mellapak 250X
reboiler temperature [°C]	120
% CO_2 removal	90
inlet temperature of flue gas stream [°C]	40
inlet temperature of free solvent [°C]	40
composition of potassium taurate solvent [M]	4 potassium hydroxide - 4 taurine
lean loading	0.19-0.30
rich loading	> 0.19-0.50

In this study, the analysis examines the potassium taurate process with and without a solid-liquid separator. In particular, sensitivity analyses have been carried out considering the effect

of changes to the lean loading, the recycle split fraction (RSF), the ΔTapproach of the lean-rich heat exchanger, and the absorber height.

1. For the lean loading sensitivity analysis, the lean loading is varied from 0.19 to 0.30 with a step size of 0.01. The analysis assumes no solid-liquid separator. The differences in temperatures between the hot inlet stream (lean solvent) and cold outlet stream (rich solvent) of the lean-rich heat exchanger is set at 10 K (Sanchez Fernandez et al., 2013).
2. For the RSF sensitivity cases, the percentage of rich liquid recycled to the absorber noted as recycle split fraction (RSF) ranges from 0.05 to 0.50, with step sizes of 0.05. The lean loading is set at 0.27.
3. For the cases examining the minimum temperature approach across the lean-rich heat exchangers, temperature differences of 1 K, 5 K and 10 K are investigated. The analysis is for lean loading values of 0.19 to 0.30, with no solid-liquid separator.
4. For the cases analyzing the absorber height, two values of removal (85% and 90%) are considered, with variation of the L/G ratios taken into account.

3. Results and Discussion

3.1. Effect of lean loading without a solid-liquid separator

The method previously described has been employed for the simulations of the process in ASPEN Plus® with a rate-based approach and for comparison with results obtained in the literature with equilibrium-based methods (Sanchez Fernandez et al., 2013).

The effect of changes in the lean loading on the solvent flowrate and the reboiler duty when a solid-liquid separator is not used are shown in Figure 2, along with results obtained by

Sanchez-Fernandez et al. (Sanchez Fernandez et al., 2013). As expected, the amount of solvent needed to accomplish the desired removal rate increases as the lean loading increases because of the decrease in the working capacity of the solvent at fixed (90%) CO_2 capture rate. The difference in the solvent flowrate obtained in this paper compared with the values reported by Sanchez-Fernandez et al. (Sanchez Fernandez et al., 2013) is because of different calcuation methods: we use kinetic-controlled reactions while Sanchez-Fernandez et al. (Sanchez Fernandez et al., 2013) use the set of chemical reactions at equilibrium.

For very lean loadings, the regenerator reduces the amount of CO_2 in the exiting solvent to a very low level by using higher stripping steam flowrate inside the column. This results in a high water / carbon dioxide ratio in the vapor phase and incurs both a high cooling duty and a high reboiler duty due to higher heat of vaporization, as shown in Figure 3a). The reboiler duty is a major operating expense of the capture plant. For higher lean loadings, the required energy per unit of solvent decreases, but a higher amount of solvent is needed to accomplish the same (fixed) carbon dioxide removal in the absorber. This imposes a lower limit on the reboiler duty per kg of carbon dioxide captured by the system. Our minimum value for the reboiler duty occurs at approximately the same lean loading (0.27) as that of Sanchez-Fernandez et al. (Sanchez Fernandez et al., 2013) (0.268), though our value is slightly higher because of the higher solvent flowrate.

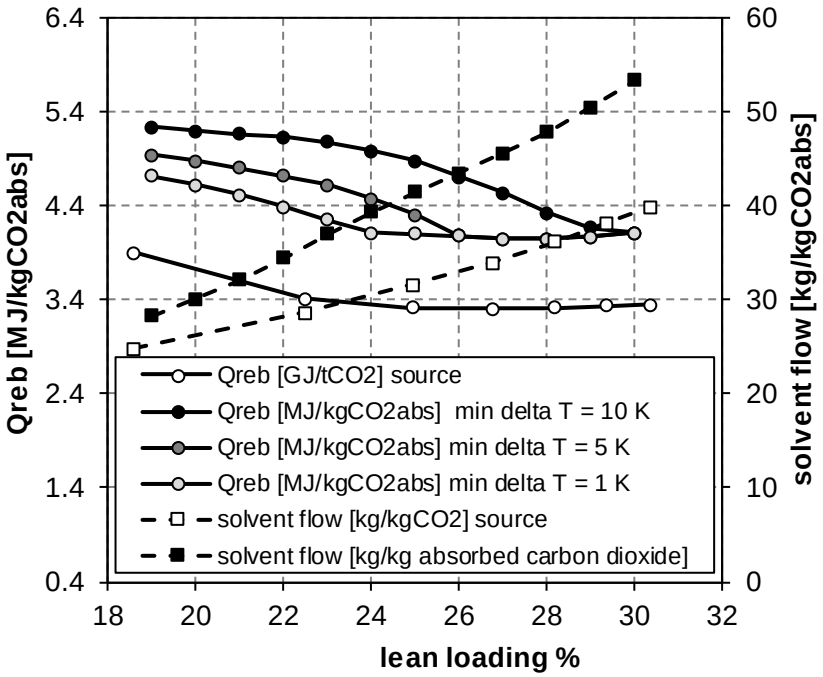

Figure 3. Variation of reboiler duty (left axis) and of solvent flowrate (right axis) vs. lean loading with no solid-liquid separator for different values of the $\Delta T_{approach}$ in the lean-rich heat exchanger. "source" refers to Sanchez-Fernandez al. (Sanchez Fernandez et al., 2013).

Figure 3 shows the breakdown in the reboiler duty for lean loadings in the range 0.19-0.30, with no solid-liquid separator. The duty is composed of three terms, *i.e.* the heat needed for desorption of carbon dioxide from the solvent (heat of desorption), the heat needed for the vaporization of water which acts as stripping steam along the column (heat of vaporization), and the heat needed for increasing the temperature of the solvent to the temperature of the reboiler (sensible heat). The relative weight of each term varies significantly as the lean loading increases, although the absolute value for the heat of desorption remains constant because of the constant capture rate in the system. The sensible heat is directly related to the solvent flowrate. It contributes about 20% of the reboiler duty for a lean loading of 0.19, but up to 45% for higher values of lean loading (>25%). The heat of vaporization is directly related to the steam stripping requirement. It contributes about 50% of the reboiler duty for a lean loading of

0.19 but this term reduces in significance as the lean loading increases, contributing less than 15% of the reboiler duty at a lean loading equal to 0.30.

a)

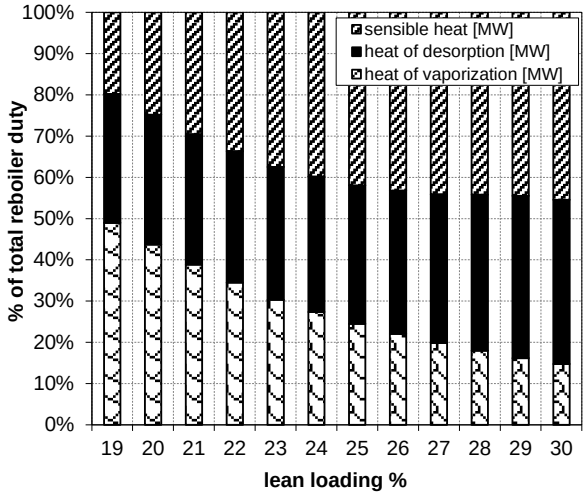

b)

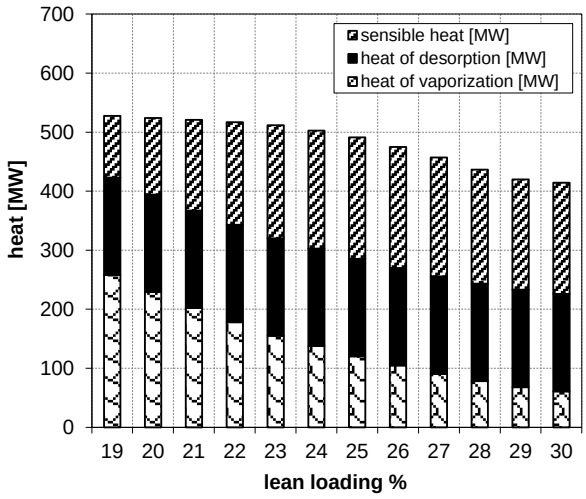

Figure 4. Breakdown of the total heat required in the reboiler for different lean loadings and RSF = 0 a) % value and b) absolute values.

Figure 4 shows the temperature profile in both the liquid and vapour phases at different locations along the absorption column for a lean loading of 0.27. Similarly to results reported

for MEA at moderate gas to liquid ratios (Plaza, 2012), the temperature profile for both phases produces a bulge, rising sharply at the bottom of the column and droping sharply at the top of the column, with a flat profile across much of the column. The temperature profile is a consequence of the phase equilibrium and the reaction kinetics, with heat being generated from the reactions of carbon dioxide with the potassium taurate solution. The temperature both influences and is influenced by the absorption rate. The height and extent of the temperature bulge depend on the ratio of liquid to vapor and also on the location in the column where most of the CO_2 is absorbed (Kohl and Nielsen, 1997). The gas (vapour) is fed to the bottom of the column at a low temperature and absorbs heat from the rich (liquid) solution, which is heated by the reactions. At the top of the column, both the liquid and vapour are cooled by the lean solvent being fed to the column. A temperature crossover occurs between the two profiles at about 40% total packing height because there is a change in heat being transferred from the liquid to the vapor at the bottom of the column to heat being transferred in the opposite direction at the top of the column.

a)

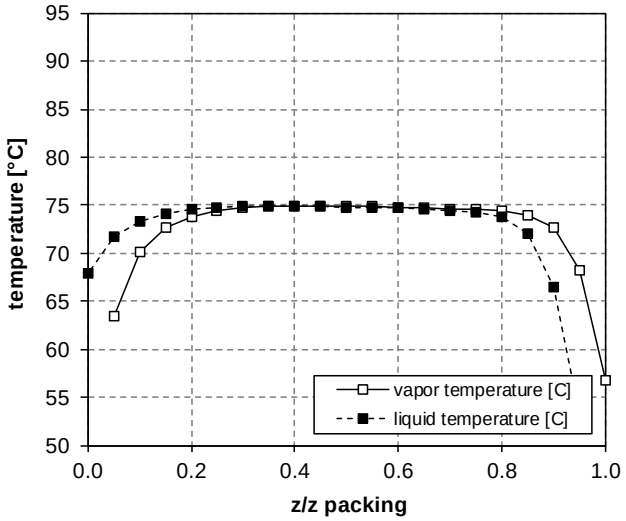

b)

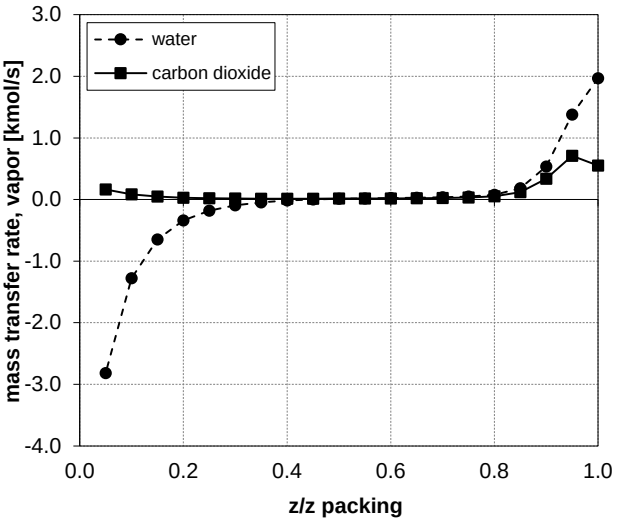

Figure 5. a) Temperature profile and b) mass transfer rate profiles along the absorption column for carbon dioxide and water for a lean loading = 0.27 and RSF = 0. Positive values indicate mass transfer from the vapor phase to the liquid phase.

This location of the temperature crossover is confirmed by an inversion in the mass transfer rate for the water vapour at the same location as shown in Figure 4b), where a positive value indicates transfer from the vapor phase to the liquid phase. Similarly to results obtained by Plaza (Plaza, 2012) for MEA, water is evaporated in the bottom part of the column and

condensed in the upper part of the column. Meanwhile, carbon dioxide only transfers via the absorption process in one direction from the vapor phase to the liquid phase. The absorption is higher close to the bottom and the top of the unit, with the highest rate occurring at 90% of the total packing height. The maximum in the absorption rate at a packing height of 95% is a result of the combined effects of temperature on the kinetics of the reactions, on the driving force and on the solubility of the carbon dioxide. The absorption rate is very low across the temperature bulge. As found previously by Rochelle (Pacheco and Rochelle, 1998) for MEA, an increase in the temperature in the column increases the kinetics but limits the reaction equilibrium, so the overall reactions are limited and thus mass transfer, which depends on the concentration difference between gas and liquid, decreases.

Figure 5 shows the profiles of the operating line and of the equilibrium curve along the entire absorber for the optimal lean loading of 0.27 for the case without the solid-liquid separator. There is a region along the absorber, at a height close to the bulge peak, where the two curves are close to each other and almost create a pinch point. The closeness of the two profiles significantly decreases the driving force for mass transfer over a significant portion of the column, leading also to the flat temperature profile at this lean loading and RSF. So the reduction in the carbon dioxide removed and reacted reduces the heat produced by the exhothermic reactions and reduces the change in temperature in the column. A very important change in the composition of the phases occurs at the top and at the bottom of the column. In these sections, the temperature is lower than in other parts of the column, so the reaction kinetics in the extreme ends of the column would most likely be lower than across the temperature bulge, but because the driving force for mass transfer is higher, a higher amount of carbon dioxide passes into the liquid phase and is absorbed.

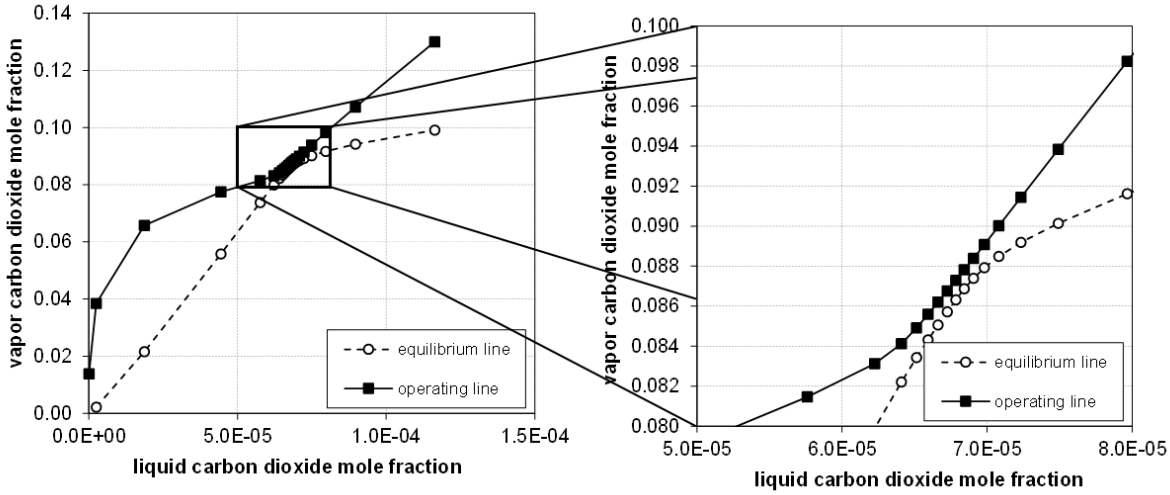

Figure 6. Operating line and of the equilibrium curve along the absorption column with a lean loading = 0.27 and RSF = 0.

Figure 6 shows the effect of lean loadings ranging from 0.19 to 0.30 on the temperature profile for the liquid phase in the absorption column. Feeding the absorption column with a lower lean loading implies that the same carbon dioxide removal rate can be achieved with a lower amount of solvent. Therefore, for a given gas flowrate, the gas to liquid ratio increases. The results show that, similarly to results reported for traditional exothermic amine solvent absorption processes by Kohl and Nielsen (Kohl and Nielsen, 1997) and by Zhang et al. (Zhang et al., 2009), increasing the lean loading (*i.e.* lowering the gas to liquid ratio) produces a flatter and lower temperature bulge across the column. At lower lean loadings (*i.e.* higher gas to liquid ratios), a profile with a distinct maximum in the temperature profile is obtained at about 80% packing height. While this profile may on first glance appear different to what has been reported for CO_2 amine absorbers (Kohl and Nielsen, 1997; Zhang et al., 2009), these nominal differences are more likely due to well known differences in the shape of the bulge caused by differences in HTCR (Heat Tansport Capacity Ratio), a ratio in which the liquid to gas ratio plays an important role, and is defined as,:

$$HTCR = \frac{Lc_P^L}{Vc_P^V} \tag{9}$$

where L and V are the liquid and vapor molar flowrates and $c^L{}_P$ and $c^V{}_P$ the heat capacities of liquid and vapor phases. For amine scrubbing systems, a detailed study of the T-bulge has been carried out by Kvamsdal and Rochelle (Kvamsdal and Rochelle, 2008), who also showed that there can be a mass transfer pinch at the temperature bulge that may reduce the mass transfer performance of the absorber. This also occurs for the system considered in this work.

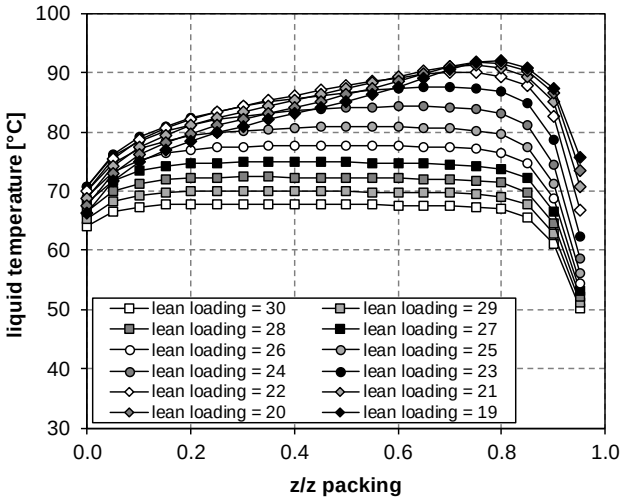

Figure 7. Temperature profile along the absorption column for different lean loadings.

Figure 7 shows the profiles obtained for the operating and equilibrium lines for a lean loading equal to 0.19. In this case, there is a less distinct approach to a pinch condition. However, the two curves get closer from around the middle to the upper part of the absorption column (corresponding to low values of mole fractions), where the temperature bulge occurs. After the temperature bulge, the column is characterized by a temperature decrease and a strong driving force for mass transfer with the highest CO_2 transfer rate occurring at the bottom of the column (Figure 8).

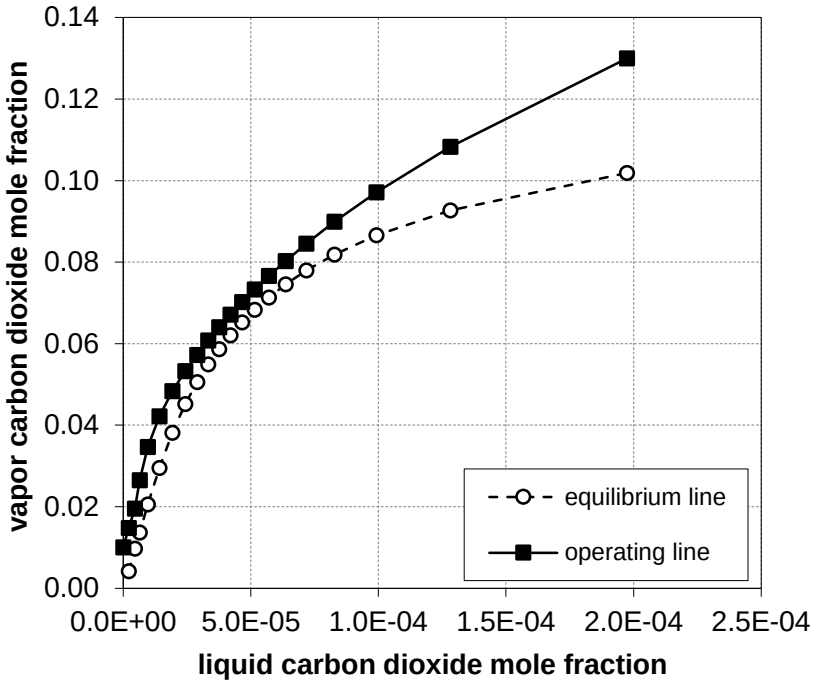

Figure 8. Profile of the operating line and of the equilibrium curve along the absorption column with a lean loading = 0.19 and RSF = 0.

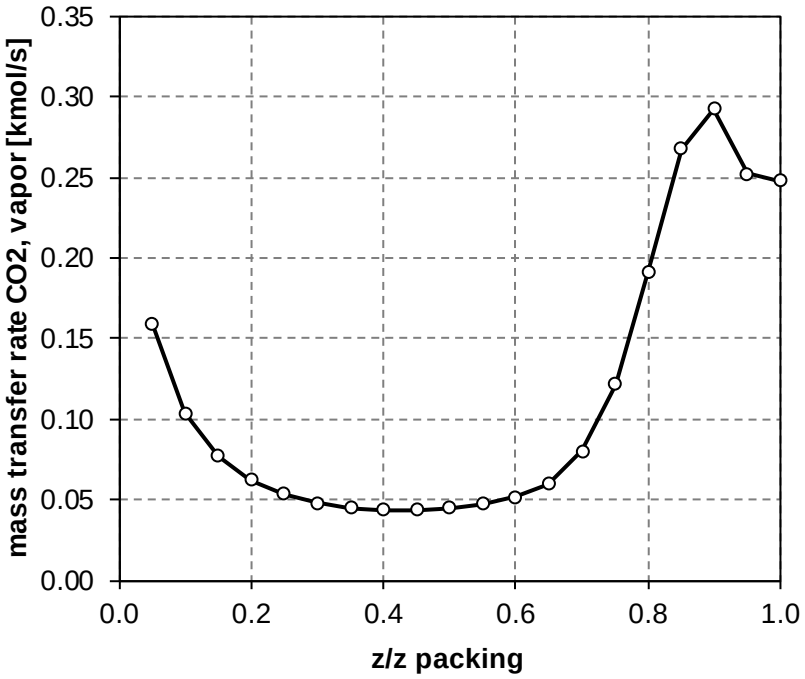

Figure 9. Profile of the mass transfer rate of carbon dioxide from the vapor phase to the liquid one along the absorption column with a lean loading = 0.19 and RSF = 0.

3.2. Effect of recycle split fraction in the solid-liquid separator

Simulations of the effect of changes in the recycle split fraction of the solid-liquid separator have been performed starting from the optimal lean loading for the scheme without the solid-liquid separator of 0.27. This value was set at the start of the simulations and then modified during the iterations.

a)

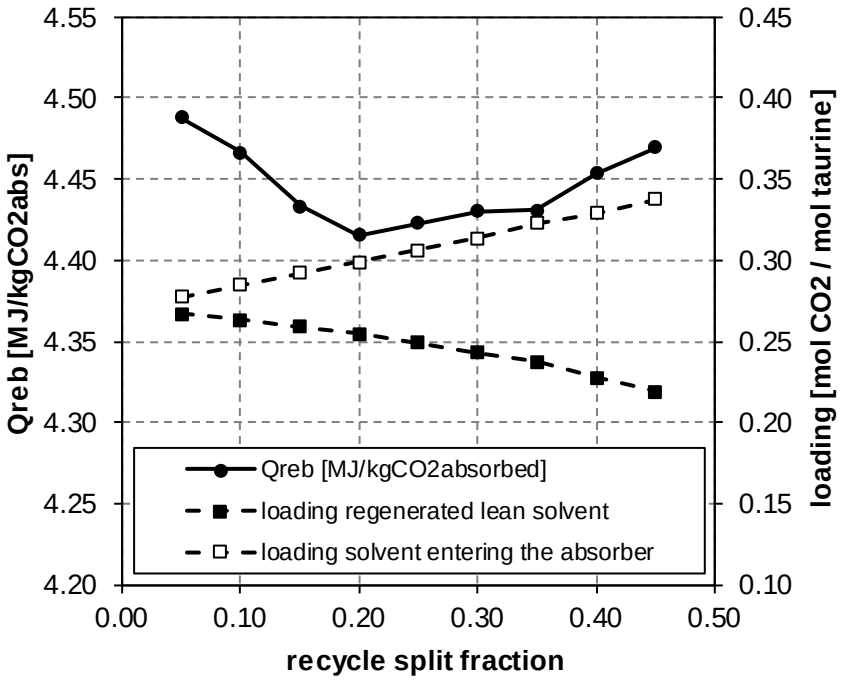

b)

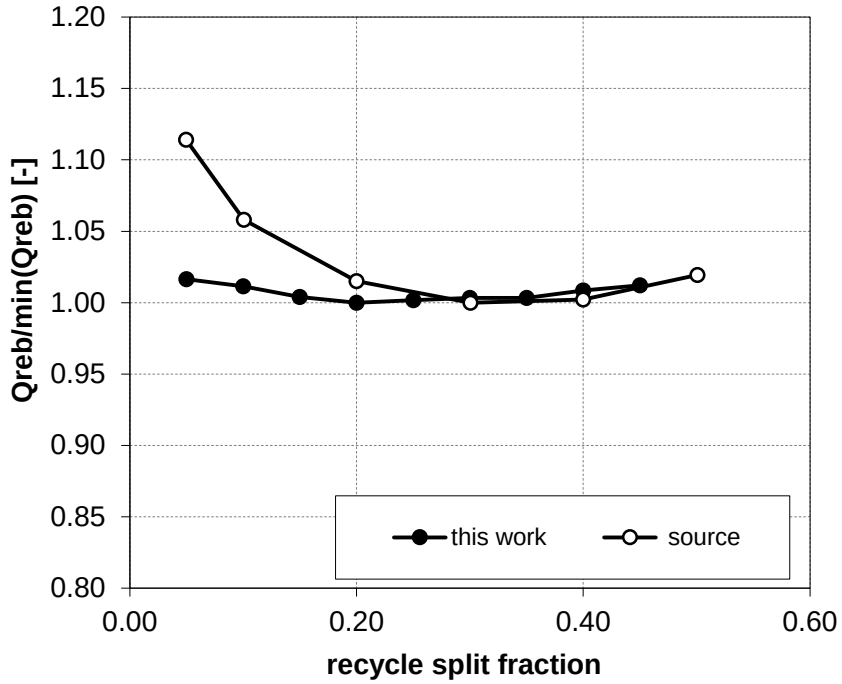

Figure 10. Variation a) of reboiler duty (left axis) and of solvent lean loading at the outlet of the regenerator and at the entrance of the absorber, after mixing with the non regenerated solvent (right axis) for different recycle split fractions, with $\Delta T_{approach}$ in the lean-rich heat exchanger equal to 10 K and b) of the ratio of reboiler duty to the minimum reboiler duty. "source" refers to Sanchez-Fernandez al. (Sanchez Fernandez et al., 2013).

The lean loading obtained at the outlet from the regenerator is different for each value of recycle split fraction considered, as shown in Figure 9a), because of the pH-shift effect. When the recycle split fraction is zero, the lean loading for the process is 0.27, however this drops to 0.22 at a recycle split fraction of 0.5. When the lean solvent stream from the regenerator and the supernatant stream from the solid-liquid separator are mixed before feeding to the absorber, an equimolar solution of taurine and potassium hydroxide is obtained. A lower lean loading is an advantage in the absorber and may help in limiting the need to increase the circulating solvent flowrate which is typical of the schemes in which a part of the non-regenerated solvent is directly recycled to the absorber. Because the recycled stream contains a high amount of

carbon dioxide, the capacity of the overall solvent decreases and a higher flowrate is generally needed to achieve a given removal of carbon dioxide.

The reboiler duty is related also to the solvent flowrate, therefore the solid-liquid separator may result in energy savings. Figure 9a) shows that the minimum reboiler duty occurs for a recycle split fraction equal to 0.20. Sanchez-Fernandez et al. (Sanchez Fernandez et al., 2013) found the optimum recycle fraction at 0.30, as shown in Figure 9b). A comparison between the trend obtained in this work and the results of Sanchez-Fernandez et al. (Sanchez Fernandez et al., 2013) shows that a flatter profile has been obtained in this work, though an optimum point is still present. This is probably the result of our fixed outlet temperature for the dissolution heat exchanger of 76°C. For higher concentrated slurries, such as the one formed after the operation of the solid-liquid separator, a higher temperature would be needed if all the solids have to be dissolved in the dissolution heat exchanger. This would result in a higher temperature of the rich stream at the entrance of the lean-rich heat exchanger, as well as a higher temperature at the entrance of the regeneration column and lower energy requirements in the reboiler. The temperature profile for the liquid phase inside the absorber for different values of the recycle split fraction is shown in Figure 10. As RSF increases, the amount of non-regenerated liquid increases and the solvent flowrate entering the absorber increases. Because the capture rate is fixed at 90%, it follows that the increase in temperature in the absorber is lower.

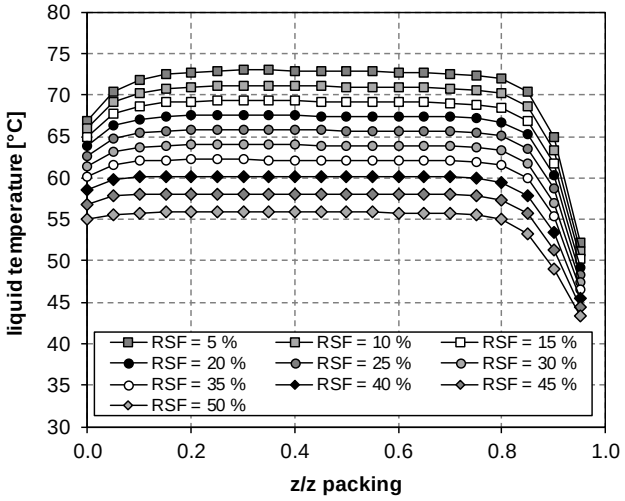

Figure 11. Temperature profile along the absorption column of the liquid phase for recycle split fractions from 5% to 50% equivalent to lean loadings of 0.27-0.35.

Figure 11 and Figure 12 show the changes in the operating and equilibrium lines along with the shift in the approach to the pinch condition for RSF = 0.20 and for RSF = 0.40, respectively. In the case of RSF = 0.20, the approach is at a vapour phase mole fraction of carbon dioxide equal to about 0.10, while in the case of RSF = 0.40 it occurs for a value higher of about 0.115. These values are also higher than the case without the solid-liquid separator, where the approach to pinch is for a value of about 0.087, *i.e.* higher in the absorber. As the recycle split fraction increases, a higher solvent flowrate is needed and therefore the temperature across the bulge decreases. This favors a lower approach to the equilibrium condition (which is always considered as the limiting condition, even when the column is simulated in rate-based mode), because the operating temperature is lower and the driving force for mass transfer is higher. The upper part of the column shows a high driving force enhanced by the increase of the slope of the equilibrium curve after the temperature cross point because of the decrease in the temperature.

The results obtained here indicate that further evaluation of factors affecting the approach to the pinch conditions and ways to avoid it may be warranted. For example, Plaza (Plaza, 2012)

have shown how intercooling can break or reduce the pinch and hence the temperature bulge for a traditional MEA absorption system.

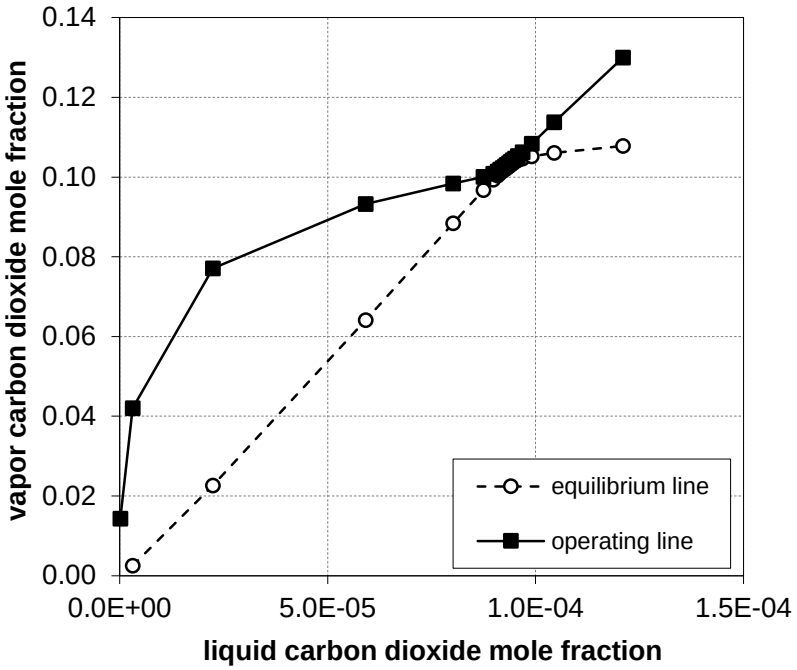

Figure 12. Profile of the operating line and of the equilibrium curve for RSF = 20.

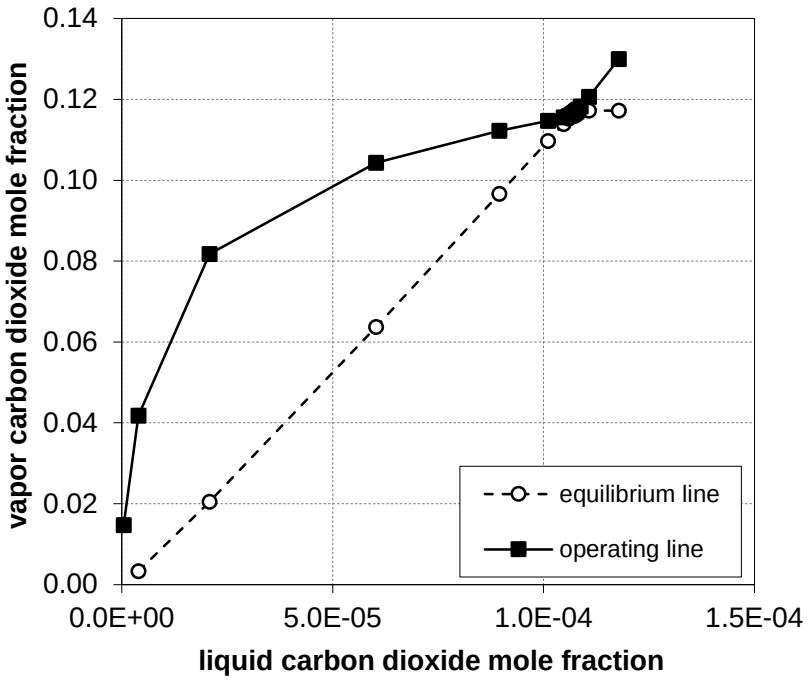

Figure 13. Profile of the operating line and of the equilibrium curve for RSF = 40.

3.3. Influence of the absorber height and L/G ratios

An analysis has been completed of the effect of the absorber height for two different values of gas to liquid ratios. To vary the G/L ratio, the gas flowrate has been maintained constant, while the liquid flowrates have been chosen so that a 90% and a 85% removal of carbon dioxide may be obtained, for the column height considered for all the other analyses as reported in Table 2.

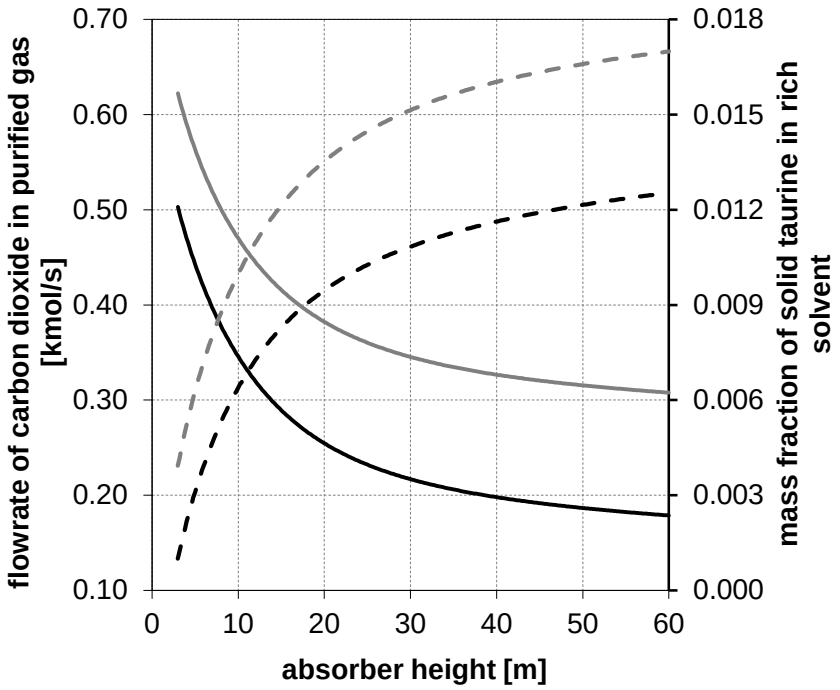

Figure 14. Flowrate of carbon dioxide gas exiting the top of the absorption column (continuous line, left axis) and mass fraction of solid taurine in the rich solution exiting the bottom of the absorption column (dotted line, right axis) for RSF = 0 with a low L/G ratio (grey curve) and a high L/G ratio (black curve) and different absorber heights.

For an initial fixed CO_2 removal and lean solvent loading, as the height of the column increases, the amount of carbon dioxide remaining in the solvent decreases and the amount of solids produced increases. As expected, increasing the column height at low column heights significantly increases the absorption, decreases the amount of CO_2 not captured and increases the amount of solids produced. However, there is a limit to the amount of CO_2 that can be removed and increasing the column height to very high values does not significantly increase CO_2 removal. Figure 13 also shows the amount of solids present in the rich solvent at the temperature of the bottom of the absorber. As the height of the column increases, the amount of solids increases. In the case of high L/G ratio the mass fraction is lower because of the higher flowrate of the solvent.

3.4. Taurine precipitation

The precipitation of solid taurine occurs in the process, and a slurry is obtained as rich solvent exiting the absorption column. This is due to the combined effects of temperature and composition of the liquid aqueous solution flowing at the bottom of the unit. Because of the rich loading, the saturation point is reached and some taurine precipitates.

The detailed composition obtained for the base scheme in terms of apparent mole and mass fractions in the liquid phase and of true mole and mass fractions of solid taurine is reported in Table 3.

Table 3. Characteristics of the lean and rich solvents, with focus on the amount of solid taurine.

stream	Lean solvent		Rich solvent	
liquid phase	**mole fraction**	**mass fraction**	**mole fraction**	**mass fraction**
carbon dioxide	0.0374	0.0483	0.04784194	0.0638999
taurine	0.1038	0.3814	0.09074066	0.34464171
potassium hydroxide	0.1038	0.1710	0.10422485	0.17746788
water	0.7550	0.3993	0.75718922	0.41398765
solid phase	**mole fraction**	**mass fraction**	**mole fraction**	**mass fraction**
taurine	0	0	0.01260283	0.04871930

4. Comparison with other solvents

A comparison of the performance (represented as reboiler duty (MJ/kg)) of the potassium taurate system with other post-combustion capture solvents is presented in Table 4. In the above baseline analysis, the absorber and regenerator dimensions were set at 20.7 m x 20 m (diameter and height) for the absorber and 16.6 m x 17.6 m for the regenerator (Table 2). In the following analysis the potassium taurate system has been specifically designed to also consider the common rules of thumbs for unit operations as absorbers and distillation columns (Turton et al., 2003; Walas, 1988). In this configuration, the absorber diameter, which strongly depends on the vapour flowrate, has been set equal to 20 m, resulting in a height of of 50 m, taking into account the generally employed maximum height of 53 m and the H/D ratio of 2.5. Similarly, the regenerator dimensions have been modified to 10.6 m for the diameter and 18 m for the height. For the scheme without a solid-liquid separator, with lean loading of 0.38 and rich loading of 0.47, this new configuration results in a reboiler duty of 2.9 MJ/kg CO_2, which is almost 30% lower than for the baseline estimates. The value could also be further reduced if the temperature approach in the lean-rich heat exchanger of 5 K is used instead of 10 K.

The results show that the energy for regeneration for the potassium taurate system in this paper has a reboiler duty lower than or comparable to that of other solvents reported in the

literature. It should be remembered that most of the other studies reported in Table 4 are for commercially advanced or well studied solvents which have incorporated process heat integration, novel designs and optimised operating conditions. This is particularly true of the MEA process, which can have baseline reboiler duties of 4.4 MJ/kg CO_2 (5M MEA), but with improved process integration has been reduced to less than 2.4 MJ/kg CO_2. This suggests that opportunities exist for improvements in the baseline potassium taurate process such as incorporating internal heat integration, split regeneration and optimisation, which could lead to further reduction in energy requirements (Ho et al., 2019)

Table 4. Reboiler duty overview reported in the literature for various postcombustion solvent processes.

Solvent		**Reboiler duty**	**CO_2 loading mol/mol**	
		(MJ/kg CO_2 captured)	Lean	Rich
Potassium Taurate	This study	2.9-4.3	0.27-0.38	0.43-0.47
MEA	(Abu-Zahra et al., 2007a; Abu-Zahra et al., 2007b; IEAGHG, 2014)	2.4-3.8	0.23	0.38
Flour econamine	(Svendsen, 2014)	3.3-3.7	-	-
KS1 (hindered amine)	(MHI, 2009)	3.3	-	-
Cansolv (Blend)	(Just, 2013)	2.4	-	-
CESAR (blend)	(Manzolini et al., 2015)·(Sanchez Fernandez et al., 2014)	3.26		
K_2CO_3	(Endo et al., 2011; Raksajati et al., 2016)	3.3-3.7	0.3	0.65
Chilled Ammonia	(Darde et al., 2012; Versteeg and Rubin, 2011)	2.4	0.3	0.66-0.68
Aqueous Ammonia	(Han et al., 2014; Yu et al., 2011)	2.5-4.2	0.17-0.19	0.35-0.4

5. Conclusion

This paper employs a rigorous rate-based model, built in the commercial process simulator ASPEN Plus®, properly customized for the representation of the system, in order to better understand the potassium taurate absorption process, by carring out detailed analyses on the performances of the system. The development of this simulation tool has allowed us to investigate some important characteristics affecting the removal of carbon dioxide including the temperature profile, the mass transfer and the operating and equilibrium lines of the absorber.

The results show that the lean loading exerts an influence not only on the capacity of the solvent, and therefore on the amount of flowrate needed to accomplish the desired separation, but also on the profiles of temperatures along the column, in addition to the energy requirements. The analysis shows that the lowest reboiler duty occurs at at lean loading of 0.27. However, operating at a lean loading of 0.27, a “pinch” condition may occur close to the temperature bulge, where the operating line and the equilibrium curve become close to one each other. Thus it is critical for effective operation to further understand the characteristics of the process such as the temperature profiles or the operating and equilibrium lines of the absorber.

The solid-liquid separator is an important unit in the potassium taurate process scheme, which includes the precipitation of taurine within the absorber section of the process. The solid-liquid separator allows part of the liquid to be separated from the slurry mixture, so that different ratios of taurine and potassium can be obtained. As the ratios change the pH also changes. This influences the partial pressure of carbon dioxide in equilibrium with the solution, which is higher if the pH is lower, and can have advantageous impacts in the regeneration section. The results suggest that recycle split fraction which results in the lowest Qreb is 0.2 (and corresponding lean loading out of stripper of 0.255).

The results show that the potassium taurate system is characterized by absorber profiles similar to those of traditional aqueous solutions. However, the precipitation of taurine has some benefits to the system in addition to low energy requirements, including a higher CO_2 loading in equilibrium with a given partial pressure of carbon dioxide and the possibility of modifying the composition of the circulating solvent by separating the solid phase.

Aknowledgement

One of the authors (S.M.) gratefully acknowledges the Australian Government for funding her research (Endeavour Research Fellowship ERF_PDR_158958_2015).

References

Abu-Zahra, M.R.M., Niederer, J.P.M., Feron, P.H.M., Versteeg, G.F., 2007a. CO_2 capture from power plants: Part II. A parametric study of the economical performance based on mono-ethanolamine. Int. J. Greenh. Gas Control 1, 135-142.

Abu-Zahra, M.R.M., Schneiders, L.H.J., Niederer, J.P.M., Feron, P.H.M., Versteeg, G.F., 2007b. CO_2 capture from power plants: Part I. A parametric study of the technical performance based on monoethanolamine. Int. J. Greenh. Gas Control 1, 37-46.

Abu Zahra, M.R.M., 2009. Carbon Dioxide Capture from Flue Gas. Development and Evaluation of Existing and Novel Process Concepts. Technische Universiteit Delft, Delft, The Netherlands.

Aftab, A., M. Shariff, A., Garg, S., Lal, B., Shaikh, M.S., Faiqa, N., 2018. Solubility of CO_2 in aqueous sodium β-alaninate: Experimental study and modeling using Kent Eisenberg model. Chem. Eng. Res. Des. 131, 385-392.

Aronu, U.E., Ciftja, A.F., Kim, I., Hartono, A., 2013. Understanding Precipitation in Amino Acid Salt systems at Process Conditions. Energy Procedia 37, 233-240.

AspenTech, 2016. ASPEN Plus® Guidelines. AspenTech, Burlington, MA.

Chen, C.C., Britt, H.I., Boston, J.F., Evans, L.B., 1979. Extension and application of the Pitzer equation for vapor-liquid equilibrium of aqueous electrolyte systems with molecular solutes. AIChE J. 25, 820-831.

Chen, C.C., Britt, H.I., Boston, J.F., Evans, L.B., 1982. Local composition model for excess Gibbs energy of electrolyte systems. Part I: single solvent, single completely dissociated electrolyte systems. AIChE J. 28, 588-596.

Chen, C.C., Evans, L.B., 1986. A local composition model for the excess Gibbs energy of aqueous electrolyte systems. AIChE J. 32, 444-454.

Copernicus, 2015. Towards a European Operational Observing System to Monitor Fossil CO_2 emissions, in: Commission, E. (Ed.).

Darde, V., Maribo-Mogensen, B., van Well, W.J.M., Stenby, E.H., Thomsen, K., 2012. Process simulation of CO_2 capture with aqueous ammonia using the Extended UNIQUAC model. Int. J. Greenh. Gas Control 10, 74-87.
Devries, N.P., 2014. CO_2 absorption into concentrated carbonate solutions with promoters at elevated temperatures. Univerisity of Illinois at Urbana-Champaign, Urbana, Illinois (USA).
Endo, K., Stevens, G., Hooper, B., Kentish, S.E., Anderson, C., 2011. A Process and Plant for Removing Acid Gases.
EPA, 2014. Air Pollution Control Technology. Fact Sheet.
Gupta, M., Coyle, I., Thambimuthu, K., 2003. CO_2 capture technologies and opportunities in Canada, Strawman document for CO_2 capture and storage (CC&S) technology roadmap, 1st Canadian CC&S TechnologyRoadmap Workshop, Calgary, Alberta, Canada.
Han, K., Ahn, C.K., Lee, M.S., 2014. Performance of an ammonia-based CO_2 capture pilot facility in iron and steel industry. Int. J. Greenh. Gas Control 27, 239-246.
Ho, M.H., Conde, E.G.C., Moioli, S., Wiley, D.E., 2019. The effect of different process configurations on the performance and cost of potassium taurate solvent absorption. Int. J. Greenh. Gas Control 81, 1-10.
IEAGHG, 2014. Techno-Economic Evaluation of Different POst Combustion CO_2 Capture Process Flow Sheet Modifications.
Just, P.-E., 2013. Advances in the development of CO_2 capture solvents. Energy Procedia 37, 314-324.
Kohl, A.L., Nielsen, R., 1997. Gas Purification, 5th ed. Gulf Publishing Company, Book Division, Houston, Texas, USA.
Kucka, L., Müller, I., Kenig, E.Y., Górak, A., 2003. On the modelling and simulation of sour gas absorption by aqueous amine solutions. Chemical Engineering Science 58, 3571-3578.
Kumar, P.S., Hogendoorn, J.A., Feron, P.H.M., Versteeg, G.F., 2001. Density, viscosity, solubility, and diffusivity of N_2O in aqueous amino acid salt solutions. J. Chem. Eng. Data 46, 1357-1361.
Kumar, P.S., Hogendoorn, J.A., Feron, P.H.M., Versteeg, G.F., 2003a. Equilibrium solubility of CO_2 in aqueous potassium taurate solutions: Part 1. Crystallization in carbon dioxide loaded aqueous salt solutions of amino acids. Ind. Eng. Chem. Res. 42, 2832-2840.
Kumar, P.S., Hogendoorn, J.A., Timmer, S.J., Feron, P.H.M., Versteeg, G.F., 2003b. Equilibrium solubility of CO_2 in aqueous potassium taurate solutions: Part 2. Experimental VLE data and model. Ind. Eng. Chem. Res. 42, 2841-2852.
Kumar, P.S., Hogendoorn, J.A., Versteeg, G.F., Feron, P.H.M., 2003c. Kinetics of the reaction of CO_2 with aqueous potassium salt of taurine and glycine. AIChE J. 49, 203-213.
Kvamsdal, H.M., Rochelle, G.T., 2008. Effects of the Temperature Bulge in CO_2 Absorption from Flue Gas by Aqueous Monoethanolamine. Ind. Eng. Chem. Res. 47, 867-875.
Lerche, B.M., 2012. CO_2 Capture from Flue gas using Amino acid salt solutions. Technical University of Denmark, Lyngby, Denmark.
Mac Dowell, N., Fennell, P.S., Shah, N., Maitland, G.C., 2017. The role of CO_2 capture and utilization in mitigating climate change. Nature Climate Change 7, 243-249.
Majchrowicz, M.E., 2014. Amino Acid Salt Solutions for Carbon Dioxide Capture. University of Twente, Twente, The Netherlands.
Majchrowicz, M.E., Brilman, D.W.F.W., Groeneved, M.J., 2009. Precipitation regime for selected amino acid salts for CO_2 capture from flue gases. Energy Procedia, 979-984.
Manzolini, G., Sanchez Fernandez, E., Rezvani, S., Macchi, E., Goetheer, E.L.V., Vlugt, T.J.H., 2015. Economic assessment of novel amine based CO_2 capture technologies integrated in power plants based on European Benchmarking Task Force methodology. Appl. Energy 138, 546-558.

Metz, B., Davidson, O., de Conik, H., Loos, M., Meyer, L., 2005. IPCC Special Report on Carbon Dioxide Capture and Storage. Prepared by Working Group III of the Intergovernmental Panel on Climate Change. Cambridge University Press, Cambridge, United Kingdom and New York, NY, USA, pp. 1-588.
MHI, 2009. Flue gas capture, 12th Meeting of the International Post-combustion CO2 Capture Network, Regina, Canada.
Mock, B., Evans, L.B., Chen, C.C., 1986. Thermodynamic Representation of Phase Equilibria of Mixed-Solvent Electrolyte Systems. AIChE J. 32, 1655-1664.
Moioli, S., Ho, M.H., Wiley, D.E., Pellegrini, L.A., 2018. Thermodynamic Modeling of the System of CO_2 and Potassium Taurate Solution for Simulation of the Process of Carbon Dioxide Removal. Chem. Eng. Res. Des. 136, 834-845.
Moioli, S., Ho, M.T., Wiley, D.E., 2017. Simulation of CO_2 Removal by Potassium Taurate Solution. Chem. Eng. Trans. 57, 1213-1218.
Moioli, S., Pellegrini, L.A., Ho, M.T., Wiley, D.E., 2019. A comparison between amino acid based solvent and traditional amine solvent processes for CO_2 removal. Chem. Eng. Res. Des.
Pacheco, M.A., Rochelle, G.T., 1998. Rate-Based Modeling of Reactive Absorption of CO_2 and H_2S into Aqueous Methyldiethanolamine. Ind. Eng. Chem. Res. 37, 4107-4117.
Perry, R.H., Green, D.W., 1997. Perry's Chemical Engineers' Handbook, 7th ed. McGraw-Hill International Editions, Singapore.
Plaza, J.M., 2012. Modeling of Carbon Dioxide Absorption Using Aqueous Monoethanolamine, Piperazine and Promoted Potassium Carbonate. The University of Texas, Austin, Texas.
Raksajati, A., Ho, M.T., Wiley, D.E., 2016. Understanding the Impact of Process Design on the Cost of CO_2 Capture for Precipitating Solvent Absorption. Ind. Eng. Chem. Res. 55, 1980-1994.
Sanchez-Fernandez, E., 2013. Novel Process Designs to Improve the Efficiency of Postombustion Carbon Dioxide Capture. Technische Universiteit Delft, Delft, The Netherlands.
Sanchez-Fernandez, E., Goetheer, E.L.V., 2011. DECAB: process development of a phase change absorption process. Energy Procedia 4, 868-875.
Sanchez Fernandez, E., Goetheer, E.L.V., Manzolini, G., Macchi, E., Rezvani, S., Vlugt, T.J.H., 2014. Thermodynamic assessment of amine based CO_2 capture technologies in power plants based on European Benchmarking Task Force methodology. Fuel 129, 318-329.
Sanchez Fernandez, E., Heffernan, K., van der Ham, L.V., Linders, M.J.G., Eggink, E., Schrama, F.N.H., Brilman, D.W.F., Goetheer, E.L.V., Vlugt, T.J.H., 2013. Conceptual Design of a Novel CO_2 Capture Process Based on Precipitating Amino Acid Solvents. Ind. Eng. Chem. Res. 52, 12223-12235.
Simons, K., Brilman, W., Mengers, H., Nijmeijer, K., Wessling, M., 2010. Kinetics of CO_2 absorption in aqueous sarcosine salt solutions: influence of concentration, temperature, and CO_2 loading. Ind. Eng. Chem. Res. 49, 9693-9702.
Svendsen, H.F., 2014. State of the art on post-combustion capture technologies, 7th Dutch CCS Symposium, Amsterdam, The Netherlands.
Turton, R., Bailie, R.C., Whiting, W.B., Shaeiwitz, J.A., 2003. Analysys, Synthesis & Design of Chemical Processes. Prentice Hall, Upper Saddle River, New Jersey, USA.
Vaidya, P.D., Konduru, P., Vaidyanathan, M., Kenig, E.Y., 2010. Kinetics of carbon dioxide removal by aqueous akaline amino acid salts. Ind. Eng. Chem. Res. 49, 11067-11072.
van Holst, J., Versteeg, G.F., Brilman, D.W.F., Hogendoorn, J.A., 2009. Kinetic study of CO_2 with various amino acid salts in aqueous solution. Chemical Engineering Science 64, 59-68.
Versteeg, P., Rubin, E.S., 2011. A technical and economic assessment of ammonia-based post-combustion CO_2 capture at coal-fired power plants. Int. J. Greenh. Gas Control 5, 1596-1605.

Walas, S.M., 1988. Chemical Process Equipment: Selection and Design. Butterworths, Stoneham, MA.
Wei, C.C., Puxty, G., Feron, P., 2014. Amino acid salts for CO_2 capture at flue gas temperatures. Chemical Engineering Science 107, 218-226.
Wei, S.C.C., Puxty, G., Feron, P., 2013. Amino acid salts for CO_2 capture at flue gas temperatures. Ghgt-11 37, 485-493.
Yu, H., Morgan, S., Allport, A., Cottrell, A., Do, T., McGregor, J., Wardhaugh, L., Feron, P., 2011. Results from trialling aqueous NH_3 based post-combustion capture in a pilot plant at Munmorah power station: Absorption. Chem. Eng. Res. Des. 89, 1204-1215.
Zhang, Y., Chen, H., Chen, C.-C., Plaza, J.M., Dugas, R., Rochelle, G.T., 2009. Rate-Based Process Modeling Study of CO_2 Capture with Aqueous Monoethanolamine Solution. Ind. Eng. Chem. Res. 48, 9233-9246.
Zhang, Z., Li, Y., Zhang, W., Wang, J., Soltanian, M.R., Olabi, A.G., 2018. Effectiveness of amino acid salt solutions in capturing CO_2: A review. Renewable and Sustainable Energy Reviews 98, 179-188.